IEICE TRANS. COMMUN., VOL.E94–B, NO.9 SEPTEMBER 2011

LETTER

Acceleration for Shadow Region Imaging Algorithm with Multiple Scattered Waves for UWB Radars

Ken AKUNE[†a)], ***Student Member***, **Shouhei KIDERA**[†], ***and*** **Tetsuo KIRIMOTO**[†], ***Members***

SUMMARY Ultra-wide band (UWB) pulse radar has high range resolution, and is thus applicable to imaging sensors for a household robot. To enhance the imaging region of UWB radar, especially for multiple objects with complex shapes, an imaging algorithm based on aperture synthesis for multiple scattered waves has been proposed. However, this algorithm has difficulty realizing in real-time processing because its computation time is long. To overcome this difficulty, this letter proposes a fast accurate algorithm for shadow region imaging by incorporating the Range Points Migration (RPM) algorithm. The results of the numerical simulation show that, while the proposed algorithm affects the performance of the shadow region imaging slightly, it does not cause significant accuracy degradation and significantly decreases the computation time by a factor of 100 compared to the conventional algorithm.

key words: *UWB radars, multiple scattered wave, RPM, shadow region imaging*

1. Introduction

UWB pulse radar with high range resolution holds great promise for the high grade imaging of objects hidden in fog or strong backlight, where optical measurements are hardly possible. This type of radar system is thus suitable for near field imaging sensors, such as rescue robots in disaster areas, or security systems designed to avoid privacy infringement. Recently, various radar algorithms aimed at high-speed and high resolution imaging have been developed, such as SEABED [1] or the RPM algorithm [2]. However, these algorithms suffer from an increased shadow region, because they employ only a single scattered signal for imaging.

Various algorithms based on a multiple scattered component have been shown to be effective in overcoming the above problem [3], [4]. Among these, an imaging algorithm based on aperture synthesis for a double scattered signal has been developed, which directly enhances the imaging range without a priori information about the target shapes or surrounding environment [5]. This algorithm synthesizes the double scattered signals along their propagation paths and reconstructs the target area, neither of which could be accomplished by previous algorithms. However, this algorithm has difficulty in real-time processing, since it requires vast computational resources as a result of multiple integrals in the synthesis process.

Manuscript received January 5, 2011.
Manuscript revised May 9, 2011.

[†]The authors are with Graduate School of Informatics and Engineering, University of Electro-Communications, Chofu-shi, 182-8585 Japan.
a) E-mail: akune@secure.ee.uec.ac.jp

DOI: 10.1587/transcom.E94.B.2696

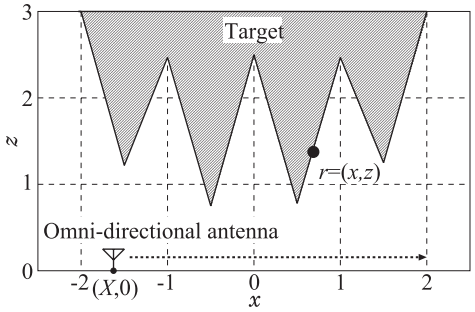

Fig. 1 System model.

To solve this problem, this letter proposes a fast accurate imaging algorithm by effectively incorporating the RPM algorithm. The proposed algorithm significantly decreases the computation burden by converting the triple integrals to single ones using Dirac's delta function determined by the target points obtained by the RPM algorithm. Numerical simulations confirm that the proposed algorithm significantly reduces the computational requirement. Moreover, although the proposed algorithm creates a different image to that by the conventional algorithm, quantitative analysis shows that it is accurate in both the target cases.

2. System Model

Figure 1 shows the system model. We assume mono-static radar and an omni-directional antenna that is scanned along the x-axis. We also assume that the target has an arbitrary shape with a clear boundary. The propagation speed of the radio wave c is also assumed to be a known constant. A mono-cycle pulse is used as the transmitting signal. The real space in which the target and antenna are located, is expressed by parameters $\boldsymbol{r} = (x, z)$ that are normalized by the central wavelength of the pulse λ. $z > 0$ is assumed for simplicity. $s'(X, Z)$ is defined as the received electric field at the antenna location $(X, 0)$, where $Z = ct/2\lambda$ is expressed by time t. $s(X, Z)$ is defined as the output of the Wiener filter with the transmitted waveform [2]. Figure 2 shows an example of $s(X, Z)$ from the complex-shaped target illustrated in Fig. 1.

3. Conventional Algorithm

SAR is a useful sensor system to observe the ground surface and for mineral resource exploration. Recently, a Synthetic

Copyright © 2011 The Institute of Electronics, Information and Communication Engineers

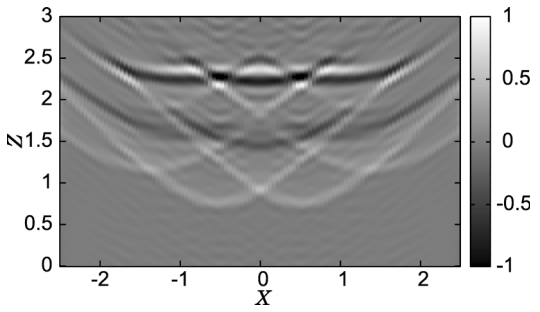

Fig. 2 Output of the Wiener filter $s(X, Z)$ from the complex-shaped target as in Fig. 1.

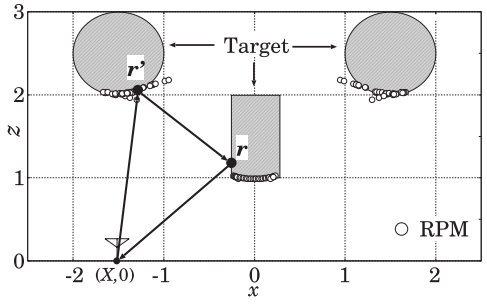

Fig. 3 Target points passed by a double scattered wave and target points with the RPM.

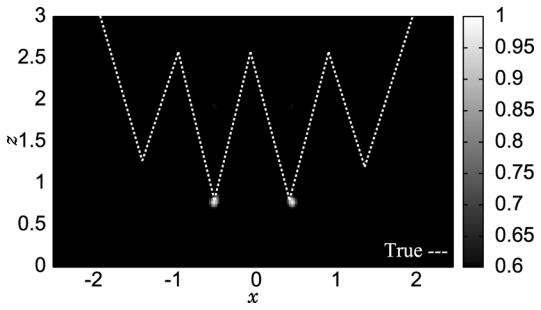

Fig. 4 Estimated image with the conventional SAR algorithm $I_1(\boldsymbol{r})$ for the complex-shaped target.

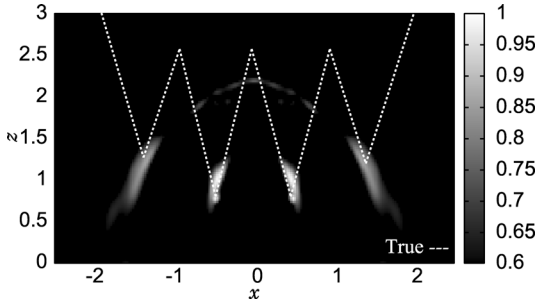

Fig. 5 Estimated image with the conventional algorithm $I^{\mathrm{S}}(\boldsymbol{r})$ for the complex-shaped target.

Aperture Radar (SAR) algorithm synthesizing the double scattered components was proposed [5], and it has been shown to enhance the imaging area remarkably by decreasing the shadow region. Figure 3 shows the example of the target points passed by a double scattered wave. This algorithm reconsiders the image $I_2^{\mathrm{S}}(\boldsymbol{r})$ using double scattered waves as

$$I_2^{\mathrm{S}}(\boldsymbol{r}) = -\int_{\boldsymbol{r}' \in R} \int_{X \in \Gamma} I_1^{\mathrm{S}}(\boldsymbol{r}')\, s\left(X, d_2(X, \boldsymbol{r}, \boldsymbol{r}')\right) \mathrm{d}X \mathrm{d}x' \mathrm{d}z', \qquad (1)$$

where $\boldsymbol{r}' = (x', z')$, R denotes the region of imaging space, Γ denotes the spatial range of the antenna scanning and $d_2(X, \boldsymbol{r}, \boldsymbol{r}') = \sqrt{(x-X)^2 + z^2} + \sqrt{(x'-X)^2 + z'^2} + \sqrt{(x-x')^2 + (z-z')^2}$. This algorithm uses negative amplitudes for $s(X, Z)$ because the phase of a double scattered wave is typically the reverse of that of a single scattered wave. $I_1^{\mathrm{S}}(\boldsymbol{r})$ as a conventional SAR image is defined as

$$I_1^{\mathrm{S}}(\boldsymbol{r}) = \int_{X \in \Gamma} s\left(X, \sqrt{(x-X)^2 + z^2}\right) \mathrm{d}X. \qquad (2)$$

Here, we assume that only the positive regions of $I_1^{\mathrm{S}}(\boldsymbol{r})$ and $I_2^{\mathrm{S}}(\boldsymbol{r})$ express the actual target boundary. The final image $I^{\mathrm{S}}(\boldsymbol{r})$ is defined as

$$I^{\mathrm{S}}(\boldsymbol{r}) = \max\left(\frac{I_1^{\mathrm{S}}(\boldsymbol{r})}{\max\left(I_1^{\mathrm{S}}(\boldsymbol{r})\right)} \ , \ \frac{I_2^{\mathrm{S}}(\boldsymbol{r})}{\max\left(I_2^{\mathrm{S}}(\boldsymbol{r})\right)} \right). \qquad (3)$$

Equation (3) highlights the image, on which $I_1^{\mathrm{S}}(\boldsymbol{r})$ or $I_2^{\mathrm{S}}(\boldsymbol{r})$ mainly focuses. This algorithm uses only the initial image $I_1^{\mathrm{S}}(\boldsymbol{r})$, and restores the target boundary where double scattered waves pass. In other words, no *a priori* knowledge about either the target shape or the surroundings is necessary to enhance the image. Figures 4 and 5 show the estimated images $I_1^{\mathrm{S}}(\boldsymbol{r})$ and $I^{\mathrm{S}}(\boldsymbol{r})$, where each signal is received at 101 locations for $-2.5 \le X \le 2.5$. Regarding $I_1^{\mathrm{S}}(\boldsymbol{r})$, $I_2^{\mathrm{S}}(\boldsymbol{r})$ and $I^{\mathrm{S}}(\boldsymbol{r})$, the number of imaging samples in each case along the x- and z-axes is set to 201 for $-2.5 \le x \le 2.5$ and $0 \le z \le 5$, respectively, with the total numbers of samples being 40401. $I^{\mathrm{S}}(\boldsymbol{r})$ increases the reconstructed region compared to the original SAR $I_1^{\mathrm{S}}(\boldsymbol{r})$. However, this algorithm has difficulty in real-time processing, since it requires vast computational resource as a result of the multiple integrals in the synthesis process. The calculation time for this algorithm is 14000 sec with a Xeon 2.40 GHz processor.

4. Proposed Algorithm

To solve the above problem, we propose a fast shadow region imaging algorithm that incorporates the RPM algorithm. The RPM algorithm accomplishes an accurate fast imaging with a single scattered wave by employing the global characteristic of so-called "range points" for accurate DOA estimation even with complex or multiple objects [2]. It should be noted that the proposed algorithm uses the target points obtained by the RPM algorithm. The RPM algorithm extracts the range points (X, Z) by detecting the local maximum of the output of the Wiener filter [2]. We also calculate the target points $\boldsymbol{r}_i = (x_i, z_i)$ corresponding to the range points (X_i, Z_i). We consider the target points from the RPM algorithm to be promising candidates for the first scat-

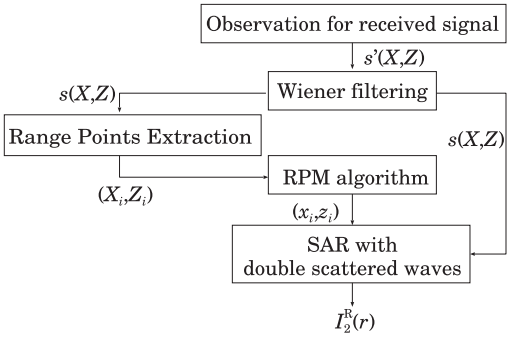

Fig. 6 Flowchart of the proposed algorithm.

tering points of double scattered waves. And then, using these points, $I_1^{\mathrm{S}}(\boldsymbol{r})$ in Eq. (1) is redefined as $I_1^{\mathrm{RPM}}(\boldsymbol{r})$,

$$I_1^{\mathrm{RPM}}(\boldsymbol{r}) = \sum_{i=1}^{N} s(X_i, Z_i) \cdot \delta(x - x_i, z - z_i), \tag{4}$$

where $\delta(*)$ is Dirac's delta function. Then, Eq. (1) degenerates to

$$I_2^{\mathrm{R}}(\boldsymbol{r}) = -\int_{X\in\Gamma} \sum_{i=1}^{N} s(X_i, Z_i)\, s(X, d_2(X, \boldsymbol{r}, \boldsymbol{r}_i))\, \mathrm{d}X. \tag{5}$$

Note that the proposed algorithm can convert the third times integral in Eq. (1) into a single integral and the summation for the number of target points estimated by the RPM algorithm. The focused final image is defined as

$$I^{\mathrm{R}}(\boldsymbol{r}) = \max\left(\frac{I_1^{\mathrm{R}}(\boldsymbol{r})}{\max\left(I_1^{\mathrm{R}}(\boldsymbol{r})\right)} \;,\; \frac{I_2^{\mathrm{R}}(\boldsymbol{r})}{\max\left(I_2^{\mathrm{R}}(\boldsymbol{r})\right)} \right), \tag{6}$$

where $I^{\mathrm{R}}(\boldsymbol{r})$ is determined by

$$I_1^{\mathrm{R}}(\boldsymbol{r}) = \sum_{i=1}^{N} s(X_i, Z_i) \cdot \exp\left(-\frac{(X - x_i)^2 + {z_i}^2}{2\sigma_{\mathrm{s}}^2} \right), \tag{7}$$

where σ_{s} is constant and empirically determined.

Figure 6 shows a flowchart of the proposed algorithm. This algorithm also suppresses false images caused by an unnecessary response due to the range sidelobe of the Wiener filter, because the RPM algorithm offers only accurate target points. Moreover, it is expected to decrease the computational requirement dramatically since all triple integrals are converted to single ones.

5. Performance Evaluation in Numerical Simulation

This section presents a performance evaluation of the conventional and proposed algorithms. Figure 7 shows the proposed images $I^{\mathrm{R}}(\boldsymbol{r})$ for a complex-shaped target, when using $s(X, Z)$ as in Fig. 2. $\sigma_{\mathrm{s}} = 0.1\lambda$ is set. The image is normalized by its maximum value. Figure 7 shows that the proposed algorithm increases the reconstructed region including on the side of the target because this algorithm suppresses unnecessary images that appear in reconstructed images using the conventional algorithm.

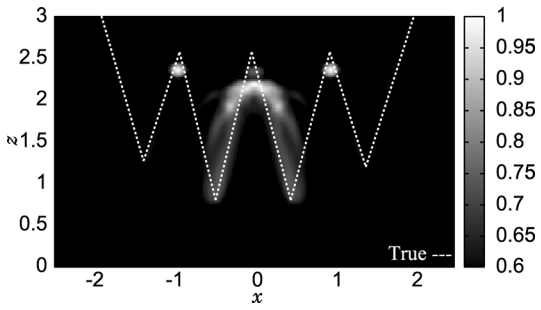

Fig. 7 Estimated image with the proposed algorithm $I^{\mathrm{R}}(\boldsymbol{r})$ for the complex-shaped target.

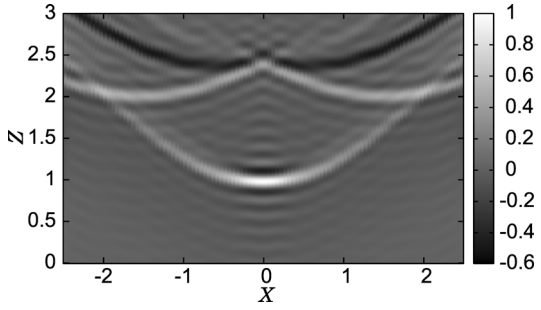

Fig. 8 Output of the Wiener filter $s(X, Z)$ from the multiple-targets.

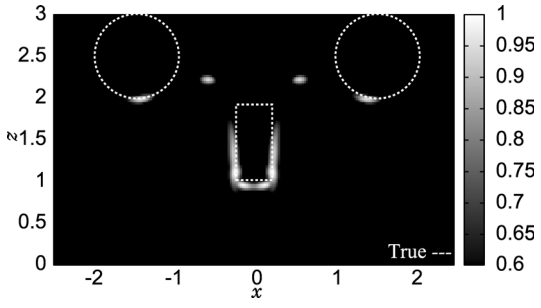

Fig. 9 Estimated image with the conventional algorithm $I^{\mathrm{S}}(\boldsymbol{r})$ for the multiple targets.

For a quantitative analysis, the evaluation value is introduced as

$$\overline{\epsilon} = \frac{\int_{\boldsymbol{r}\in R} \min_{\boldsymbol{p}_{\mathrm{true}}} \left\| \boldsymbol{r} - \boldsymbol{p}_{\mathrm{true}} \right\| |I(\boldsymbol{r})|\, \mathrm{d}\boldsymbol{r}}{\int_{\boldsymbol{r}\in R} |I(\boldsymbol{r})|\, \mathrm{d}\boldsymbol{r}}, \tag{8}$$

where $\boldsymbol{p}_{\mathrm{true}}$ are the true target points. Here, min $(*)$ denotes the minimizing operation and $\|*\|$ is the Euclidean norm. This evaluation value denotes the accuracy weighted by the image intensity. The evaluation shows that 0.0782λ for the conventional algorithm, and 0.0148λ for the proposed algorithm. This result shows quantitatively that the proposed algorithm has a significant advantage in accurate imaging. It should be noted that the calculation times for the proposed and conventional algorithms are within 125 s, and 14000 s, respectively, using a Xeon 2.40 GHz. That is, the proposed algorithm decreases the calculation time by around 100 times. This is because N in the proposed algo-

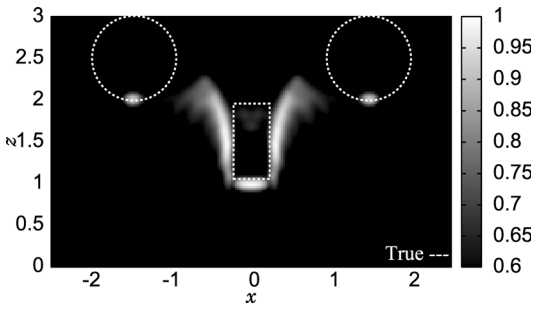

Fig. 10 Estimated image with the proposed algorithm $I^{\mathrm{R}}(\boldsymbol{r})$ for the multiple targets.

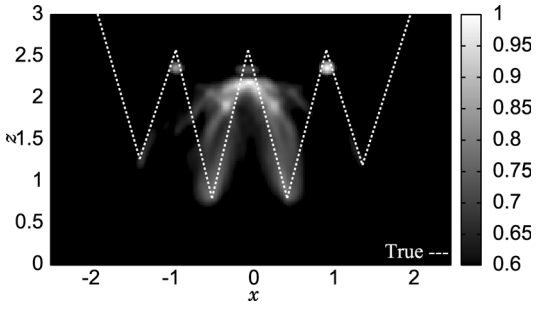

Fig. 11 Estimated image with the proposed algorithm $I^{\mathrm{R}}(\boldsymbol{r})$ for the complex-shaped target in noisy case at S/N=35 dB.

rithm is reduced to 124 from 40401, which is the equivalent number used in the conventional algorithm. Furthermore, Fig. 8 shows $s(X, Z)$ from the multiple targets illustrated in Fig. 3. Figures 9 and 10 show the conventional and proposed images $I^{\mathrm{S}}(\boldsymbol{r})$ and $I^{\mathrm{R}}(\boldsymbol{r})$ for Fig. 3, respectively, when using $s(X, Z)$ as in Fig. 8. $\sigma_{\mathrm{s}} = 0.1$ is set. The evaluation value shows 0.0712λ for the conventional algorithm and 0.116λ for the proposed algorithm. This result shows quantitatively that the proposed algorithm achieves accuracy around of 0.1 λ. While this accuracy is slightly worse than that of the conventional algorithm, the proposed algorithm substantially enhances the imaging range making it possible to recognize the rectangular side. It should also be noted that the calculation times for the proposed and conventional algorithms are within 120 s and 14000 s, respectively, using a Xeon 2.40 GHz. The number of target points, N, for the RPM is 145, which is significantly less than the equivalent number used in the conventional algorithm, that is, 40401.

Finally, we evaluate the performance through a noisy simulation. Gaussian white noise is added to $s'(X, Z)$. S/N is defined as the ratio of peak instantaneous signal power to the average noise power after applying the matched filter. Figures 11 and 12 show estimated images with the proposed algorithm for a complex-shaped target and multiple targets, respectively. The S/N ratios are 35 dB for Fig. 11 and 15 dB for Fig. 12. Figure 11 shows that the proposed algorithm also enhances the imaging range, although false images due to the random noise components appear above

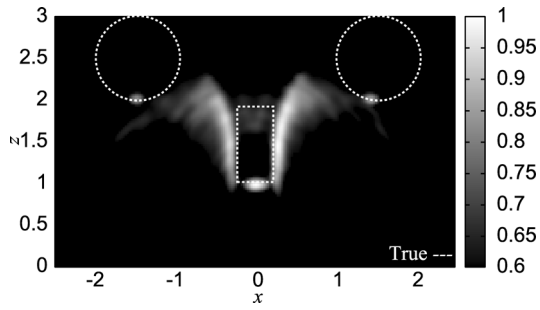

Fig. 12 Estimated image with the proposed algorithm $I^{\mathrm{R}}(\boldsymbol{r})$ for the multiple targets in noisy case at S/N=15 dB.

the actual boundary. This is because the random noise is mostly suppressed in the synthesis process. Figure 12 shows that the magnitude of the focused images is relatively weak compared to that in the noiseless case. However, the evaluation result shows 0.0197λ for Fig. 11 and 0.282λ for Fig. 12. These results show that the proposed algorithm is capable of maintaining its performance in noisy situations.

6. Conclusion

This letter proposed a fast imaging algorithm for a double scattered wave by making use of the target points created by the RPM algorithm. The conventional algorithm suffers from the problem of requiring large computational resources, because it employs multiple integrals in the synthesis process. The proposed algorithm uses Dirac's delta function to efficiently decrease the multiple integration, determined by the target points from the RPM algorithm, thereby significantly decreasing the computational cost. It has been shown that the calculation time for the proposed algorithm is reduced about 100 times. Note that, although the proposed algorithm generally produces a different image to that obtained by the conventional algorithm, quantitative analysis has verified that there is no fatal accuracy degradation in the case of either target.

References

[1] T. Sakamoto and T. Sato, "A target shape estimation algorithm for pulse radar systems based on boundary scattering transform," IEICE Trans. Commun., vol.E87-B, no.5, pp.1357–1365, May 2004.
[2] S. Kidera, T. Sakamoto, and T. Sato, "Accurate UWB Radar 3-D imaging algorithm for complex boundary without wavefront connections," IEEE Trans. Geosci. Remote Sens., vol.48, no.4, pp.1993–2004, April 2010.
[3] S.K. Lehmanm and A.J. Devaney, "Transmission mode time-reversal super-resolution imaging," Acoust. Soc. Am., vol.113, no.5, May 2003.
[4] J.M.F. Moura and Y. Jin, "Detection by time reversal: Single antenna," IEEE Trans. Signal Process., vol.55, no.1, pp.187–201, Jan. 2007.
[5] S. Kidera, T. Sakamoto, and T. Sato, "Shadow region imaging algorithm based on aperture synthesis with multiple scattered waves for UWB radars," Proc. PIERS 2009, vol.5, no.4, pp.393–396, Aug. 2009.